Supporting Information

Cassago et al. 10.1073/pnas.1112495109

SI Materials and Methods

Tissue Array Analysis. Human normal and tumor breast tissue arrays containing 10 cases of adjacent normal and normal tissue, 20 fibroadenoma, 10 lobular carcinoma, 30 infiltrating ductal carcinoma, and 10 matched mets of breast in lymph nodes (BR8010, U.S. Biomax) or 75 cases of different grades of invasive ductal breast tumors and 16 adjacent and nonadjacent normal tissue (BR1921, U.S. Biomax) were subjected to immunohystochemical analysis with KGA and GAC antibodies. The tissue array slides were deparaffinized by baking at 60 °C for 30 min and then rehydrated in distilled water containing 3% H_2O_2 for 30 min. After washing with PBS, the slides were boiled for 10 min in 10 mM sodium citrate buffer (pH 6.0) and allowed to cool to room temperature. The slides were then blocked with 2.5% horse serum and with Avidin and Biotin blocking solutions (Avidin/Biotin Blocking Kit; Vector Labs). The tissue arrays were incubated with the primary antibodies followed by biotinylated secondary antibodies, and treated for 30 min with the Elite ABC reagent (Universal R.T.U. Vectastain Elite ABC Kit; Vector Labs). After washing with PBS, the slides were processed with chromogen solution (ImmPACT DAB Substrate; Vector Labs). The slides were then dehydrated and mounted. The resulting staining obtained with each antibody was quantified using Image J software.

Immunoblotting, Immunofluorescence, and Immunoprecipitation. Cells were lysed with 25 mM Tris-HCl pH 8.0, 100 mM NaCl, 1% Triton X-100, 1 mM EDTA, 1 mM DTT, 1 mM $NaVO^4$, 1 mM β-glycerol phosphate, 11 $\mu g.mL^{-1}$ aprotinin, 11 $\mu g.mL^{-1}$ pepstatin and 1 mM PMSF. The lysates were resolved by SDS-PAGE, and the proteins transferred to polyvinylidene fluoride membranes. The membranes were incubated overnight with the primary antibodies diluted in 20 mM Tris, 135 mM NaCl and 0.02% Tween 20. The primary antibodies were detected with horseradish peroxidase-conjugated secondary antibodies followed by exposure to ECL reagent (Pierce). PageRuler Prestained Protein Ladder Plus was used (Fermentas). For immunofluorescence studies, SKBR3 cells were seeded in a 384 wells Cell Carrier plate (Perkin Elmer) and left to attach for 16 h 37 °C with 5% of CO_2. Cells were fixated and permeabilized with 3.7% Formaldehyde in PBS/0.2% Triton X-100, blocked with 3% BSA in PBS/0.8% Triton X-100, and incubated for 16 h, 4 °C, with 2.5 ng/mL KGA antibody diluted in 3% BSA in PBS/0.8% Triton X-100. Goat secondary antimouse—FITC (Sigma-Aldrich), diluted in blocking solution (1:200) was used to reveal KGA cell location. Nuclei and mitochondria were stained with 2.5 $\mu g.mL^{-1}$ DAPI (Sigma) and 500 nM MitoTracker Red CMXRos(Invitrogen), respectively. Data were collected with the plate-reader Fluorescence Microscope Operetta (Perkin Elmer). For the immunoprecipitation assays, 500 μg of cell lysate transfected or not with pcDNA-hKGA-V5 (Invitrogen), kindly provided by Dr. Richard Cerione, were added to 6 μg of antiKGA (Abnova) overnight at 4 °C. Next day, the mixture was added to 30 μL of Dynabeads Protein G (Invitrogen), incubated for 4 h at 4 °C and then washed three times with 200 μL of 50 mM Tris-HCl pH 8.0 and 150 mM NaCl. Washed beads were boiled with SDS-PAGE loading sample, resolved by SDS-PAGE and immunobloted with 1:5,000 monoclonal mouse anti-V5 (Invitrogen).

Protein Expression and Purification. The rat KGA gene (residues Met128-Leu674) cloned in pET15b was previously published by the laboratory of Norman Curthoys (9). Equivalent constructs of GAC (Met128-Ser603) and LGA (Leu72-Val602) were amplified from a mouse fetal brain tissue cDNA library and cloned into the pET28a plasmid (Novagen). The following expression and purification protocol was applied to the three mammalian glutaminase constructs, transformed into *Escherichia coli* Rosetta-2 thermocompent cells (Merck). Overnight cultures, grown in LB medium in the presence of 50 $\mu g.mL^{-1}$ kanamycin and 50 $\mu g.mL^{-1}$ cloramphenicol, were inoculated in a ratio of 1:200 in 4 L cultures supplemented with the same antibiotics and left shaking at 250 rpm for 5 h at 37 °C. The cultures were then down-tempered to 18 °C for 1 h before induction with 1 mM IPTG (isopropyl β-D-1-thiogalactopyranoside) for 5 h at 25 °C. Cells were collected by rapid centrifugation and resuspended in 500 mM NaCl, 50 mM Tris-HCl pH 8.5, 10% glycerol and 2 mM BME (β-mercaptoethanol), added with bacterial protesase inhibitors. Cell lysis was performed chemically, by incubation with hen egg-white lysozyme, DNAse I and deoxycholate (all three reagents from Sigma-Aldrich) for about 1 h, incubated on ice. The soluble fractions were separated from the debris by high speed centrifugation and subsequently loaded, by gravity and in a cold room, on Co^{2+}-charged resin TALON (Clontech), previously equilibrated with the running buffer 10 mM NaCl, 50 mM Tris-HCl pH 8.5 and 2 mM BME. The constructs, bearing a His-tag fused to their N terminus, were eluted stepwise using running buffer to which up to 500 mM imidazole (vol/vol) had been added. The tag was then removed by overnight digestion with bovine thrombin (Sigma-Aldrich) and the samples loaded into a MonoQ anion exchange chromatography column (GE Healthcare). Elution was done by performing a linear gradient with a buffer containing 1 M NaCl, 50 mM Tris-HCl pH 8.5 and 2 mM Dithiothreitol and the fractions containing the proteins of interest were loaded in a Superdex 200 10/30 size-exclusion column (GE Healthcare), equilibrated with 500 mM NaCl, 30 mM TRIS-HCl pH 8.5 and 0.5 mM TCEP [tris(2-carboxyethyl)phosphine)]. Protein concentration was determined by UV 280 nm using calculated extinction coefficients.

Glutaminase Activity. The validation of the Glutaminase-GDH-coupled assay can be found in Table S2 and Fig. S2*A*. In order to obtain the kinetic paramenters for the recombinant wild-type glutaminases, as well as for the point mutants, a mix containing 5 nM glutaminase, 50 mM Tris-acetate pH 8.6, 3 units of bovine L-Glutamate Dehydrogenase (Sigma-Aldrich), 2 mM NAD (Sigma-Aldrich) was pipetted into 96-well plates previously filled with 6 or 12 serial dilutions of L-glutamine, to achieve a range of concentrations from 60 mM to 0.15 mM. For the assays performed in the presence of phosphate ions, K_2HPO_4 (2 M stock, pH 9.4) was added to the mix at final concentrations of 1, 5, 10, 20, and 50 mM. The formation of NADH was tracked by absorbance readings at 340 nm, for up to five consecutive minutes, at room temperature. Measurements were done in triplicate. The initial velocities, in picomols of NADH produced per second, were calculated using an extinction coefficient for NADH of 6,220 $M^{-1}.cm^{-1}$ at 340 nm and 0.5 cm of path length. The total volume per reaction was 200 microliters. Plate-reader used was either an EnSpire (Perkin Elmer) or an Infinite 200 (Tecan). Measurements were done in triplicates and analyzed using GraphPad Prism 5.00 (GraphPad Software, San Diego California) and Microcal Origin 8.1 (Microcal Software, Inc., Northampton, USA). We thank Dr. Fábio Squina and Dr. Roberto Ruller (CTBE/CNPEM) for accessibility to the TECAN plate-reader.

Size-Exclusion Analysis of Serial Dilutions. Size-exclusion chromatography was performed on a Superdex 200 HR 10/30 column (GE) in 30 mM Tris-HCl pH 8.0, 100 mM NaCl (or 500 mM when

indicated), 0.5 mM TCEP [tris(2-carboxyethyl)phosphine)], at a flux of 0.5 mL. min^{-1}. For Stokes radii calculations, the column was previously calibrated with the Molecular Weight Calibration Kit (Sigma).

Crystallization. Glutaminase C (GAC) resultant from the size-exclusion purification step was concentrated down with an Amicon ultrafiltration device (100 KDa cutoff; Millipore) to a final concentration of approximately 3.3 mg/mL. Crystallization experiments were performed at 291 K using the conventional sitting drop vapor diffusion technique. Drops were made by mixing three parts of protein to one of well solution, containing 17% PEG 3350, 0.2 M NaCl and 0.1 M Bis-Tris pH 6.5. Clusters of plates were observed after 2 d and used as seeds for standard streak-seeding in a mother-liquor solution containing 13% PEG 3350, 0.2 M NaCl and 0.1 M Bis-Tris pH 6.5. Before data collection at cryogenic temperature (100 K), harvested crystals were cryoprotected with 15% ethylene glycol added to the mother-liquor. For the crystal structure obtained in the presence of phosphate ions, 40 mM K_2HPO_4 was added (vol/vol) to the protein solution prior to crystallization and left in incubated on ice by at least 1 h. The same incubation protocol was applied to the third set of crystals, grown in the presence of glutamate (10 mM final concentration). All the subsequent steps, including the seeding, were the same as for the apo protein crystals.

X-Ray Crystallography. Data were processed using Mosflm (1) and merged and scaled with SCALA (2). The first set of phases was obtained by the molecular replacement technique as implemented in the program Phaser (3), using the dataset from the apo crystals, and searching for four monomers in the asymmetric unit, as predicted from the Matthews coefficient (4). The crystal structure of the active site portion of the human glutaminase was used as the search model [PDB code 3CZD (†)]. After the MR procedure, density modification was performed using the program Parrot, which is part of the CCP4 suite (†, 6) and the improved map then submitted to automated interpretation by the ARPwARP routine (7). Positional and *B*-factor refinement cycles were carried out with Phenix (8). Manual building of the extra portions and real space refinement, including Fourier electron density map inspection, were performed with COOT (9). Solvent water molecules, treated as oxygen atoms, were added using the appropriate COOT routine. For the isomorphous phosphate bound crystals, a monomer from the ligand-free structure was used as phasing model. Due to intrinsic lower resolution limitations, non-crystallographic symmetry restraints were used during refinement up until the final stages of refinement. During model refinement, the inspection of Fourier difference maps indicated the presence of very strong nonprotein electron densities (over 3σ in height in the F_{obs}-F_{calc} Fourier maps) inside the canonical active site of each one of the three distinct crystalline models. Due to their sizes and shapes, and in respect with the crystallization condition, they were readily identified as a chloride ion in the apo crystals (3ss3), a phosphate ion (3ss4) and L-glutamate (3ss5), and subsequently refined as such. The overall stereochemical quality of the final models and the agreements between them and experimental data were assessed by the program Molprobit (10) and the appropriate COOT routines. Electrostatic potential surface mapping was performed by APBS (11).

Small Angle X-Ray Scattering (SAXS) Data Collection and Processing. Scattering data were collected at a wavelength $\lambda = 1.488$ Å, for sample-detector distances of 1.1 m covering the momentum transfer ranges $0.015 < s < 0.442$ $Å^{-1}$ ($s = 4\pi \sin\theta/\lambda$, where 2θ is the scattering angle). The data were normalized to the intensity of the incident beam and corrected for the detector response using an in-house program. In order to check for radiation damage in the sample, two frames of 250 s were collected and compared using the program PRIMUS (12). The same program was used to average the frames and subtract the buffer. The different protein concentrations were evaluated for aggregation by following increases in the measured *Rg* (radius of gyration) as calculated by autoRg. The *Rg* was confirmed by using the indirect Fourier transform program GNOM (13, S14), which was also used to calculate the distribution function $P(r)$ and *D* max. The data was analyzed and processed using the programs contained in the ATSAS package (15). Ab initio construction was performed by GASBOR (16). The models (twenty in total) were averaged and filtered by DAMAVER (17) and superposed to the crystallographic structure using SUPCOMB (18).

†Karlberg T, et al. (2008) Still to be published. Coordinate file and structure factors available at www.rcsb.org, under code 3czd.

1. Leslie AG (1992) Recent changes to the MOSFLM package for processing film and image plate data. *Joint CCP4 + ESF-EAMCB Newsletter on Protein Crystallography* 26:27–33.
2. Evans PR (2005) Scaling and assessment of data quality. *Acta Crystallographica Section D* 62:72–82.
3. McCoy AJ, et al. (2007) Phaser Crystallographic software. *J Appl Cryst* 40:658–674.
4. Matthews BW (1968) Solvent content of protein crystals. *J Mol Biol* 33:491–497.
5. Zhang KY, Cowtan K, Main P (1997) Combining constraints for electron-density modification. *Methods in Enzymology* 277:53–64.
6. Collaborative Computational Project, Number 4 (1994) The CCP4 Suite: programs for protein crystallography. *Acta Crystallographica Section D* 50:760–763.
7. Perrakis A, Morris RM, Lamzin VS (1999) Automated protein model building combined with iterative structure refinement. *Nature Struct Biol* 6:458–463.
8. Adams PD, et al. (2010) *PHENIX*: a comprehensive Python-based system for macromolecular structure solution. *Acta Crystallographica Section D* 66:213–221.
9. Emsley P, Lohkamp B, Scott WG, Cowtan KP (2010) Features and development of COOT. *Acta Crystallographica Section D* 66:486–501.
10. Chen VB, et al. (2010) MolProbity: all-atom structure validation for macromolecular crystallography. *Acta Crystallographica Section D* 66:12–21.
11. Baker NA, Sept D, Joseph S, Holst MJ, McCammon JA (2001) Electrostatics of nanosystems: application to microtubules and the ribosome. *Proc Natl Acad Sci USA* 98:10037–10041.
12. Konarev PV, Volkov VV, Sokolova AV, Koch MH, Svergun DI (2003) PRIMUS: a Windows PC-based system for small-angle scattering data analysis. *J Appl Crystallogr* 36:1277–1282.
13. Svergun DI (1991) Mathematical methods in small-angle scattering data analysis. *J Appl Crystallogr* 24:485–492.
14. Svergun DI (1992) Determination of the regularization parameter in indirect-transform methods using perceptual criteria. *J Appl Crystallogr* 25:495–503.
15. Petoukhov MV, Konarev PV, Kikhney AG, Svergun DI (2007) ATSAS 2.1—towards automated and web-supported small-angle scattering data analysis. *J Appl Cryst* 40:223–228.
16. Svergun DI, Petoukhov MV, Koch MH (2001) Determination of domain structure of proteins from X-ray solution scattering. *Biophys J* 80:2946–2953.
17. Volkov VV, Svergun DI (2003) Uniqueness of ab initio shape determination in small-angle scattering. *J Appl Cryst* 36:860–864.
18. Kozin M, Svergun DI (2000) Automated matching of high- and low-resolution structural models. *J Appl Cryst* 34:33–41.

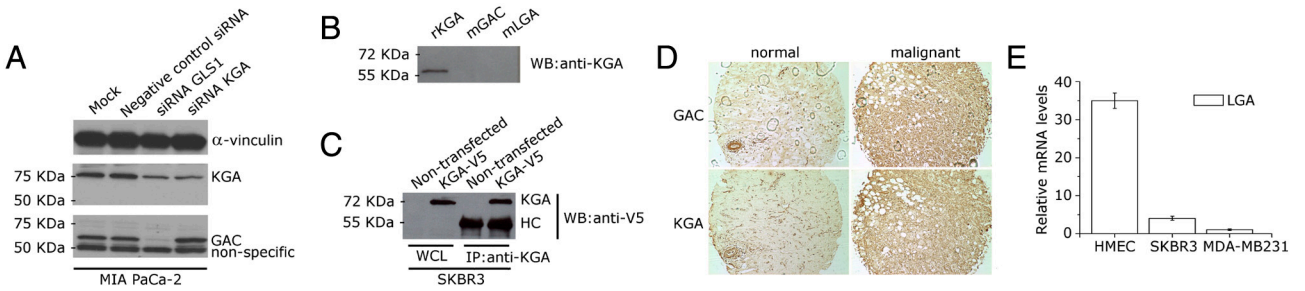

Fig. S1. (*A*) KGA and GAC knock down was carried out using Stealth Select RNAi duplex (Invitrogen) directed against either the two isoforms of GLS1 (GCUAAUGGUGGUUUCUGCCCAAUUA) or specifically the KGA (GAGCAGCGGGAUUAUGACUCCAGAA) isoform. The siRNA oligonucleotides were transiently transfected in MIA PaCa-2 pancreatic cell line using Lipofectamine 2000 (Invitrogen) and the relative knock down efficiency was determined using monoclonal KGA specific antibody (Abnova; clone 5C4) and peptide affinity-purified polyclonal GAC antibody (custom-ordered for this project from Genscript). A scrambled siRNA was used as a negative control and MOCK received only the Lipofectamine 2000 reagent. Molecular marker used was Precision Plus Protein Kaleidoscope standards (Biorad). (*B*) Antibody antiKGA (Abnova) can specifically recognize 100 ng of recombinant rat KGA (rKGA) but not 100 ng of recombinant mouse GAC or LGA (mGAC or mKGA) on an immunoblotting assay. Molecular marker used was Precision Plus Protein Dual Color standards (Biorad). (*C*) Immunoprecipitation assay of SKBR3 cells transfected with human full length KGA, kindly provided by Dr. Richard Cerione (pcDNA3.1-V5, Invitrogen) using antiKGA (Abnova) antibody followed by immunoblotting with anti-V5 (Invitrogen) revealed that antiKGA can immunoprecipitate ectopic hKGA. WCL is short for Whole Cell Lysate and HC is the short for Immunoglobulin Heavy Chain. Molecular marker used was Precision Plus Protein Dual Color standards (Biorad). (*D*) Representative immunohistochemistry data for consecutive slices of human breast normal and cancer tissue array samples. (*E*) qPCR experiment were performed using ABI 7500 Fast Real-Time PCR System (Applied Biosystems) and Power SYBRGreen PCR Master Mix following the fabricant specifications. Total RNA was extracted from the cell lines using the kit RNeasy (Qiagen) and cDNA synthesis accomplished with Superscript III cDNA synthesis kit (Invitrogen). For LGA amplification we used the sequences: Forward—5′GAAATTCGGAACAAGACTGTG 3′; Reverse—5′AACTTCGATGTGTCCTTCAC 3′. The 18S ribosomal RNA was used as housekeeping gene for the normalization (Forward—5′ATTCCGATAACGAACGAGAC 3′ and Reverse—5′TCACAGACCTGTTATTGCTC 3′). Values are given as amplification fold relative to MDA-MB 231.

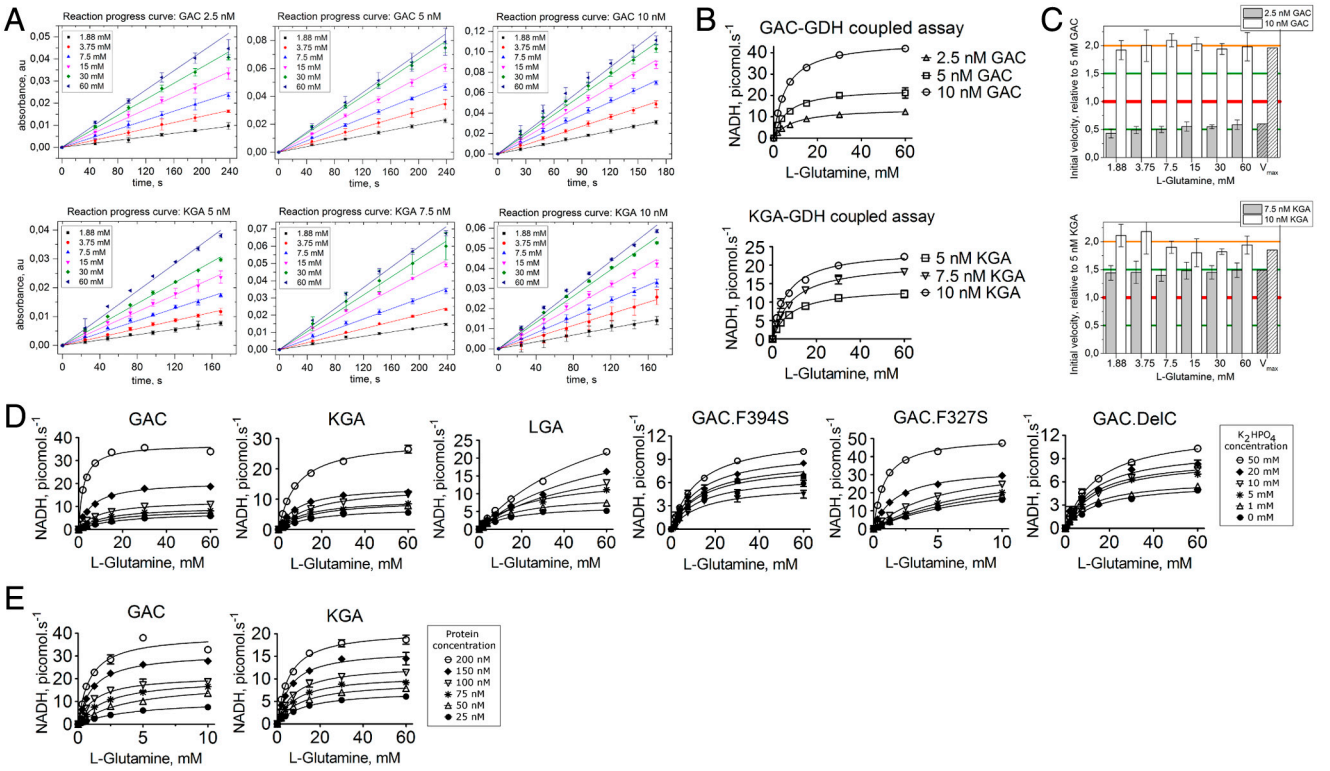

Fig. S2. Validation of the GDH-coupled enzymatic assay and kinetic curves of the recombinant glutaminase isozymes GAC, KGA and LGA, as well as for the GAC point and deletional mutants. (*A*) By plotting the raw kinetic data subtracted by the background readings, obtained in the presence of 20 mM phosphate buffer, we show that the formation of NADH proceeds at rates which are linear with time and dependent only on the concentration of the glutaminases for the time measured. (*B*) GAC and KGA Michaelis-Menten curves as a function of different concentrations of GAC (2.5, 5, and 10 nM) and KGA (5, 7.5, and 10 nM). (*C*) The proportionality of the initial velocities can be seen when half, three-halves and double the amount of glutaminases are used (either GAC or KGA), against different substrate concentrations. (*D*) Michaelis-Menten curves as a function of increasing concentrations of inorganic phosphate for wild-type GAC, KGA, and LGA, as well as for GAC point mutants F394S and F327S and deletional mutant DelC. (*E*) Michaelis-Menten curves as a function of protein concentration for the wild-type GAC and KGA.

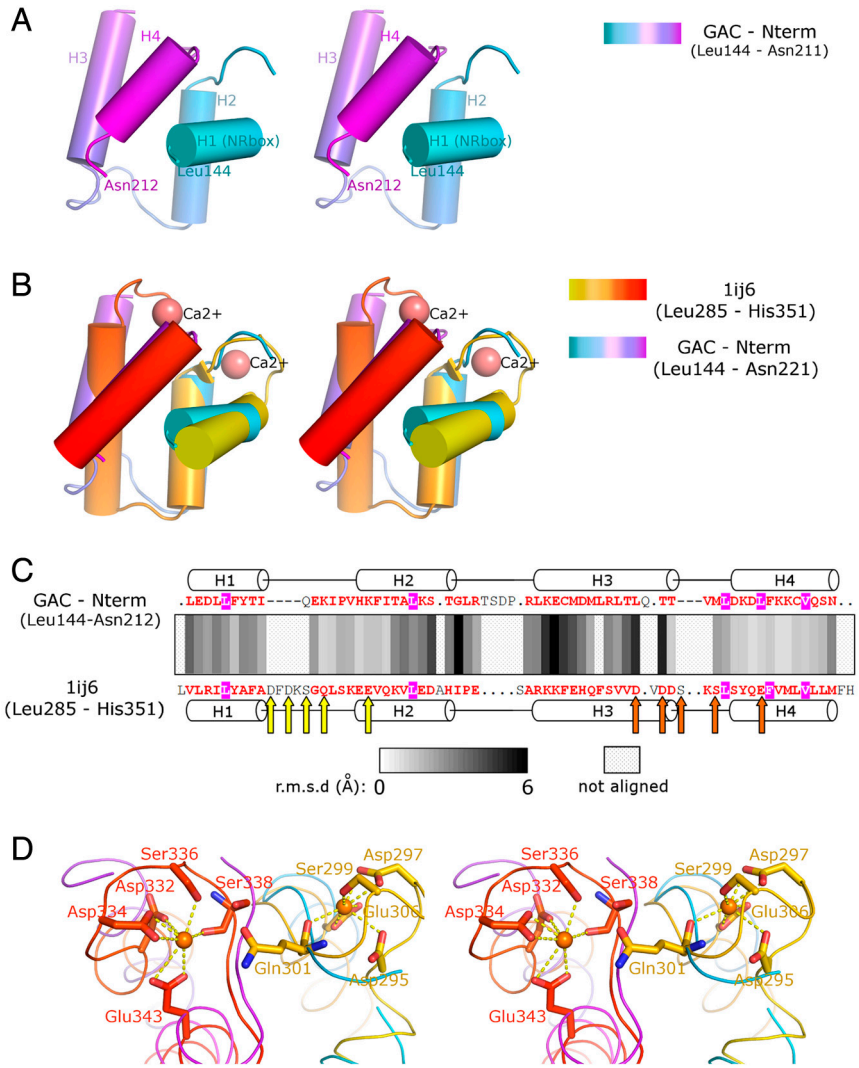

Fig. S3. The structure of the N-terminal portion of GAC. (*A*) Stereographic view of the structure of N-terminal portion of Glutaminase C (spanning residues Leu144 to Asn221), which folds into a unicornate helix-bundle (1). The amphipatic LXXLL motif (commonly termed the NR box, short for Nuclear Receptor box, where X is any amino acid) is identified between residues Leu144 to Leu148. NR boxes participate in many protein-protein interactions associated with different aspects of transcriptional regulation of nuclear receptor coregulators (2). It is also reported the need for oppositely charged residues flanking this motif, allowing complementary charge interactions with the receptor (3). This condition is also fulfilled in GAC, where positively and negatively charged residues (Lys135/Lys137 and Glu154/Glu157) prevail amino- and carboxy-terminal to the core sequence, respectively. (*B*) According to the DALI server (4), the N-terminal region of GAC has the calmodulin domain of plasmodial specific Lav1-1 protein (PDB code 1ij6, Z-score and rmsd of 5.9 and 2.9 Å, respectively) as the closest structural match, though with only 10% sequence identity (*C*). rmsd is plotted as a function of residue number, according to alignment. Orange and yellow arrows indicate residues that participate in the coordination of the two calcium ions found in 1ij6. These residues can be seen graphically in (*D*). Neither these residues nor an appropriate environment for cation coordination is found in the N-terminal of GAC. LSQMAN (5) and O2D (6) were used to produce (*C*).

1 Harris NL, Presnell SR, Cohen FE (1994) Four helix-bundle diversity in globular proteins. *J Mol Biol* 236:1356–1368.
2 Plevin MJ, Mills MM, Ikura M (2005) The LXXLL motif: a multifunctional binding sequence in transcriptional regulation. *Trends in Biochemical Sciences* 30:66–69.
3 Bramlett KS, Wu Burris TP (2001) Ligands specify coactivator nuclear receptor (NR) box affinity for estrogen receptor subtypes. *Molecular Endocrinology* 15:909–922.
4 Holm L, Rosenström P (2010) Dali server: conservation mapping in 3D. *Nucl Acids Res* 38:545–549.
5 Kleywegt GJ, Jones TA (1994) A super position.*CCP4/ESF-EACBM Newsletter Protein Crystallography* 31:9–14.
6 Kleywegt GJ (1997) Les amis d'O. *CCP4/ESF-EACBM Newsletter Protein Crystallography* 34:5–8.

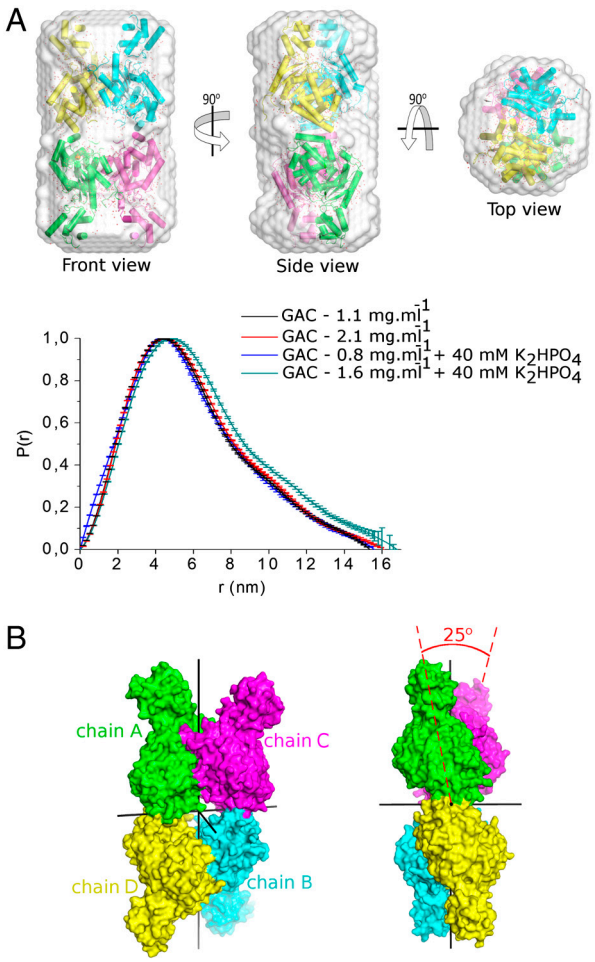

Fig. S4. (*A*) In the higher box, orthogonal views of the superposition between the SAXS envelope for GAC, as eluted from the size-exclusion purification step, and its X-ray crystal structure, showing high correlation between the tetramer assembly in solution and in the crystal. Pair-distance distribution function distribution function, $P(r)$, obtained for GAC subject to SAXS experiments, at different protein concentrations, indicating no signs of protein aggregation and conservation of the tetramer assembly, in the presence and absence of 40 mM phosphate. (*B*) D2 symmetry of the Glutaminase C tetramer. The dimer comprising chains A and D is twisted of about 25° in respect to the one comprising chains B and C, along the shortest axis of the oligomer.

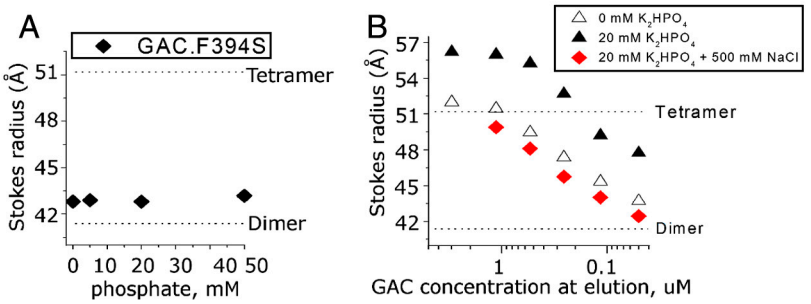

Fig. S5. (*A*) The GAC.F394S mutant was assayed for its capacity to form tetramers by size-exclusion chromatography, and the result showed that this mutation was enough to break the tetramer into dimers, even in the presence of high phosphate concentrations, as opposed to what is observed for the wild-type GAC (Fig. 4*C* in the main text). (*B*) Serial dilution profile of GAC in the presence of 500 mM NaCl, indicating the chloride, which competes with Pi for binding to the catalytic Ser291, as observed in our crystal structures, at high enough concentration can dislodge phosphate from its site and shift the protein equilibrium to lower-order oligomers.

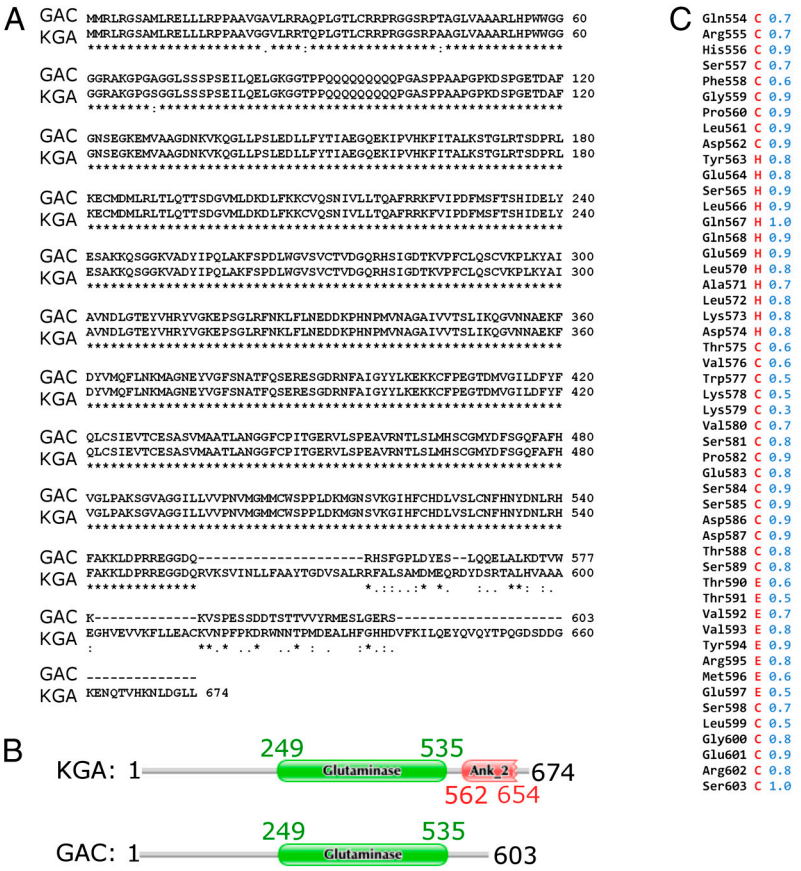

Fig. S6. Sequence-based analysis of GAC and KGA. (*A*) Primary sequence alignment performed by ClustalW (1), using NCBI reference sequences NP_001106854 (mouse GAC, *Mus musculus*) and AAA41247.1 (rat KGA, *Rattus norvegicus*), showing virtually complete identity from Met1 up to Gln554. The splicing event that differentiates both kidney-type isoforms, gives origin to very unique C terminii (from Gln554 onwards), where only 12% sequence identity is found, between GAC and KGA. (*B*) Besides the glutaminase domain on both isoforms (green box), the Pfam database (2) predicts three ankyrin repeats in KGA C-terminal region (red box), spanning residues Leu562 to Gln654. No functional domains or motifs are predicted for the equivalent region in GAC. (*C*) Secondary structure prediction, by APSSP2 server (3), suggests the presence of short α-helix (from Tyr563 to Asp574) and a extended strand (spanning residues Thr590 to Glu597), all permeated by random coil (red letters stand for H = helix, E = Strand and C = Coil). Blue numbers indicate probability of correct prediction.

1 Thompson JD, Higgins DG, Gibson TJ (1994) CLUSTAL W: improving the sensitivity of progressive multiple sequence alignment through sequence weighting, positions-specific gap penalties and weight matrix choice. *Nucleic Acids Research* 22:467–4680.

2 Finn RD, et al. (2010) The Pfam protein families database. *Nucleic Acids Research* 38:D211–D222.

3 Raghava GP (2000) Protein secondary structure prediction using nearest neighbor and neural network approach. *CASP* 4:75–76.

Table S1. Kinetic parameters for the wild-type glutaminases and the GAC point mutants, as measured in the coupled assay

			$K_{m\text{-app}}$ (mM)			
Pi (mM)	GAC	KGA	LGA	GAC.F394S	GAC.F327S	GAC.DelC
0	18.40 ± 2.10	15.60 ± 1.90	15.20 ± 2.00	13.96 ± 2.88	8.24 ± 0.89	14.39 ± 1.98
1	14.05 ± 1.30	15.80 ± 1.40	17.30 ± 1.90	13.39 ± 1.59	8.97 ± 0.67	12.02 ± 1.05
5	11.70 ± 0.80	12.60 ± 0.77	23.80 ± 2.30	13.17 ± 1.21	7.77 ± 0. 42	14.55 ± 1.82
10	9.20 ± 0.62	15.80 ± 1.20	40.20 ± 5.90	13.24 ± 1.72	5.02 ± 0.07	12.93 ± 1.70
20	5.70 ± 0.33	9.00 ± 0.40	53.80 ± 7.10	13.07 ± 1.48	1.72 ± 0.07	13.34 ± 2.07
50	2.10 ± 0.15	8.45 ± 0.50	60.50 ± 6.50	12.33 ± 0.75	0.84 ± 0.03	14.79 ± 0.93
			$k_{cat\text{-app}}$ (s^{-1})			
Pi (mM)	GAC	KGA	LGA	GAC.F394S	GAC.F327S	GAC.DelC
0	7.75 ± 0.35	7.20 ± 0.31	6.85 ± 0.34	5.76 ± 0.45	29.57 ± 1.82	5.94 ± 0.31
1	8.92 ± 0.32	9.89 ± 0.34	9.60 ± 0.43	7.01 ± 0.31	34.80 ± 1.52	6.28 ± 0.19
5	9.88 ± 0.24	10.10 ± 0.28	15.09 ± 0.64	8.45 ± 0.29	35.93 ± 1.09	9.05 ± 0.43
10	13.00 ± 0.45	14.39 ± 0.43	21.1 ± 1.66	9.01 ± 0.44	36.66 ± 1.40	9.15 ± 0.44
20	20.62 ± 0.34	14.44 ± 0.26	29.90 ± 2.32	10.24 ± 0.43	33.96 ± 0.52	10.30 ± 0.59
50	37.05 ± 0.49	29.65 ± 0.56	43.14 ± 2.79	12.18 ± 0.27	51.06 ± 0.8	12.81 ± 0.31
			$k_{cat\text{-app}}/K_{m\text{-app}}$ ($mM^{-1}.s^{-1}$)			
Pi (mM)	GAC	KGA	LGA	GAC.F394S	GAC.F327S	GAC.DelC
0	0.42 ± 0.07	0.46 ± 0.08	0.45 ± 0.08	0.41 ± 0.09	3.59 ± 0.43	0.41 ± 0.03
1	0.63 ± 0.08	0.63 ± 0.08	0.55 ± 0.09	0.53 ± 0.07	3.88 ± 0.31	0.52 ± 0.03
5	0.84 ± 0.08	0.80 ± 0.07	0.63 ± 0.09	0.64 ± 0.07	4.62 ± 0.29	0.62 ± 0.05
10	1.41 ± 0.14	0.91 ± 0.10	0.52 ± 0.12	0.68 ± 0.10	7.3 ± 0.64	0.71 ± 0.44
20	3.62 ± 0.27	1.60 ± 0.10	0.56 ± 0.13	0.78 ± 0.10	19.74 ± 1.07	0.77 ± 0.08
50	17.64 ± 1.50	3.50 ± 0.27	0.71 ± 0.12	0.99 ± 0.08	60.80 ± 2.62	0.87 ± 0.04

Table S2. Validation of the Glutaminase-GDH-coupled assay

Glutaminase C (GAC)

Initial velocity

	2.5 nM GAC		5 nM GAC		10 nM GAC	
L-Glutamine Substrate, mM	v_0, au.s^{-1} ($\times 10^{-5}$)	NADH* v_0, picomol.s^{-1}	v_0, au.s^{-1} ($\times 10^{-5}$)	NADH* v_0, picomol.s^{-1}	v_0, au.s^{-1} ($\times 10^{-5}$)	NADH* v_0, picomol.s^{-1}
1.88	4.1 ± 0.4	2.6 ± 0.3	9.42 ± 0.8	6.1 ± 0.5	18.2 ± 0.2	11.7 ± 0.1
3.75	6.9 ± 0.3	4.5 ± 0.2	14.37 ± 1.2	9.2 ± 0.8	28.1 ± 1.5	18.4 ± 1.0
7.5	9.7 ± 0.6	6.3 ± 0.4	19.68 ± 0.9	12.6 ± 0.6	41.1 ± 0.3	26.4 ± 0.2
15	13.9 ± 1.3	9.0 ± 0.9	25.33 ± 1.2	16.3 ± 0.8	51.5 ± 0.4	33.1 ± 0.3
30	17.1 ± 0.5	11.0 ± 0.3	31.30 ± 1.1	20.1 ± 0.7	60.6 ± 0.9	39.0 ± 0.6
60	19.2 ± 0.7	12.4 ± 0.4	32.94 ± 3.7	21.2 ± 2.4	65.3 ± 1.0	42.0 ± 0.6

Kinetic parameters—GAC

2.5 nM GAC		5 nM GAC		10 nM GAC	
V_{max}, picomol.s^{-1}	$k_{cat\text{-app}}$, s^{-1}	V_{max}, picomol.s^{-1}	$k_{cat\text{-app}}$, s^{-1}	V_{max}, picomol.s^{-1}	$k_{cat\text{-app}}$, s^{-1}
14.2	28.3 ± 0.6	23.4	23.4 ± 0.6	45.9	22.9 ± 0.1

Kidney-type Glutaminase (KGA)

Initial velocity

	5 nM KGA		7.5 nM KGA		10 nM KGA	
L-Glutamine Substrate, mM	v_0, au.s^{-1} ($\times 10^{-5}$)	NADH* v_0, picomol.s^{-1}	v_0, au.s^{-1} ($\times 10^{-5}$)	NADH* v_0, picomol.s^{-1}	v_0, au.s^{-1} ($\times 10^{-5}$)	NADH* v_0, picomol.s^{-1}
1.88	4.2 ± 0.2	2.7 ± 0.1	9.42 ± 0.8	3.9 ± 0.2	8.8 ± 0.4	5.7 ± 0.1
3.75	6.9 ± 0.5	4.4 ± 0.3	14.37 ± 1.2	6.4 ± 0.2	14.9 ± 2.2	9.6 ± 1.3
7.5	10.1 ± 0.5	6.5 ± 0.3	19.68 ± 0.9	9.1 ± 0.3	19.3 ± 0.3	12.4 ± 0.2
15	13.8 ± 1.2	8.9 ± 0.9	25.33 ± 1.2	13.2 ± 0.2	24.9 ± 1.3	16.0 ± 0.8
30	17.3 ± 0.2	11.1 ± 0.1	31.30 ± 1.1	16.1 ± 1.2	30.9 ± 0.5	19.9 ± 0.3
60	20.9 ± 1.6	12.2 ± 1.0	32.94 ± 3.7	18.2 ± 0.1	36.1 ± 0.3	23.7 ± 0.2

Kinetic parameters—KGA

5 nM KGA		7.5 nM KGA		10 nM KGA	
V_{max}, picomol.s^{-1}	$k_{cat\text{-app}}$, s^{-1}	V_{max}, picomol.s^{-1}	$k_{cat\text{-app}}$, s^{-1}	V_{max}, picomol.s^{-1}	$k_{cat\text{-app}}$, s^{-1}
13.9	13.9 ± 0.3	20.8	13.9 ± 0.4	24.2	12.1 ± 0.2

*The initial velocity, in picomols of NADH produced per second, was calculated using an extinction coefficient for NADH of 6,220 $M^{-1}.cm^{-1}$ at 340 nm (1) and 0.5 cm of path length. The total volume per reaction was 200 microliters.

1 Dawson RB (1985) *Data for biochemical research* (3rd ed.). (Clarendon Press, Oxford).

Table S3. X-ray crystallography data collection parameters and structure refinement statistics

	Data collection		
	3ss3(GAC ligand-free form)	3ss4(GAC PO_4-bound form)	3ss5(GAC L-Glu-bound form)
Beamline	X12-C at NSLS	F-1 at CHESS	W02B-MX2 at LNLS
Space group	$P2_12_12_1$	$P2_12_12_1$	$P12_11$
Cell parameters a, b, c (Å)	99.3, 138.8, 179.5	97.7, 136.3, 176.1	50.4, 139.4, 178.4 $\beta = 93.8°$
Resolution range (Å)	20.0–2.42 (2.55–2.42)	38.5–2.85 (3.00–2.85)	42.9–2.80 (2.95–2.80)
Unique reflections	89,075 (12,230)	51,943 (7,247)	59,822 (8,638)
Redundancy	4.2 (3.7)	3.5 (3.1)	2.3 (2.2)
R_{symm} (%)	14.4 (61.6)	15.2 (62.6)	10.6 (43.1)
Completeness (%)	94.2 (89.5)	94.2 (91.0)	99.0 (98.7)
$I/\sigma(I)$	5.8 (1.8)	5.1 (1.7)	6.0 (1.7)
Average mosaicity (°)	0.92	0.99	0.85
B-factor from Wilson Plot (Å^2)	38.4	64.0	64.2
Monomers/AU	4	4	4
Solvent content (%)	57.7	55.4	58.2
Matthews coeff. (A^3/Da)	2.91	2.76	2.94
	Refinement		
Resolution range (Å)	20.0–2.42	20.0–2.85	20.0–2.80
Reflections (cross-validation*)	88,926 (4,439)	51,693 (2,631)	59,611 (3,013)
R_{factor}/R_{free} (%)	19.5/25.0	22.7/26.9	20.6/24.0
Average *B*-factor/rmsd (Å^2)			
Main chain (no. of residues)	29.5/2.8 (1,552)	45.4/3.5 (1,559)	44.7/3.2 (1,575)
Side chain (no. of residues)	32.9/4.2 (1,350)	47.9/5.2 (1,360)	46.7/4.6 (1,369)
Ligand (no. of molecules)	29.7/4.8 (4)	57.8/3.1 (4)	49.8/2.7 (4)
Solvent (no. of molecules)	34.8/8.5 (1,105)	35.5/7.3 (255)	37.7/6.6 (214)
rmsd from standard geometry			
Bond length (Å)	0.006	0.013	0.03
Bond angles (°)	1.090	1.021	0.708
Ramachandran plot			
Most favored (%)	97.5	96.7	97.0
Allowed (%)	2.1	2.7	2.5
Outlier (%)	0.4	0.6	0.5

*Data for outer shell shown in parentheses. Cross-validation test set size of 5%.